

Size-resolved global emission inventory of primary particulate matter from energy-related combustion sources[☆]



E. Winijkul^a, F. Yan^{a,*}, Z. Lu^a, D.G. Streets^a, T.C. Bond^b, Y. Zhao^c

^a Energy Systems Division, Argonne National Laboratory, Argonne, IL 60439, USA

^b Department of Civil and Environmental Engineering, University of Illinois at Urbana-Champaign, Urbana, IL 61801, USA

^c School of the Environment, Nanjing University, Nanjing 210046, PR China

HIGHLIGHTS

- Mass-based size distribution of emissions of energy-related combustion sources.
- Method to estimate the size distribution of components of the combustion sector.
- Global PM₁₀ emissions showing single-mode size distribution with peak around 700 nm.
- Discussion of uncertainties in global size distribution emission estimation.
- Investigation of mass size distribution changes with emission reduction scenarios.

ARTICLE INFO

Article history:

Received 3 September 2014

Received in revised form

9 February 2015

Accepted 12 February 2015

Available online 13 February 2015

Keywords:

Mass size distribution

PM emissions

Combustion sources

Global size-resolved emission inventory

ABSTRACT

Current emission inventories provide information about the mass emissions of different chemical species from different emitting sources without information concerning the size distribution of primary particulate matter (PM). The size distribution information, however, is an important input into chemical transport models that determine the fate of PM and its impacts on climate and public health. At present, models usually make rather rudimentary assumptions about the size distribution of primary PM emissions in their model inputs. In this study, we develop a global and regional, size-resolved, mass emission inventory of primary PM emissions from source-specific combustion components of the residential, industrial, power, and transportation sectors for the year 2010. Uncertainties in the emission profiles are also provided. The global size-resolved PM emissions show a distribution with a single peak and the majority of the mass of particles in size ranges smaller than 1 μm . The PM size distributions for different sectors and world regions vary considerably, due to the different combustion characteristics. Typically, the sizes of particles decrease in the order: power sector > industrial sector > residential sector > transportation sector. Three emission scenarios are applied to the baseline distributions to study the likely changes in size distribution of emissions as clean technologies are implemented.

© 2015 Published by Elsevier Ltd.

1. Introduction

Knowledge of the size distribution of aerosols is essential to

understanding climate and human health effects. Aerosol optical properties depend strongly on the size distribution (Haywood and Boucher, 2000; Yu et al., 2006); and sub-micrometer aerosols, which have longer atmospheric lifetimes, scatter more light per unit mass (Seinfeld and Pandis, 2006). Smaller carbonaceous aerosols lead to larger, more negative, direct and indirect aerosol forcing (Bauer et al., 2010). The number of cloud condensation nuclei (CCN) per mass of aerosol depends on the chemical composition of aerosols as a function of size (Anttila et al., 2012; Feingold, 2003; McFiggans et al., 2006). In addition, it is well known that the size distribution of particulate matter (PM) determines the potential for human health effects; small particles can

[☆] The submitted manuscript has been created by UChicago Argonne, LLC, Operator of Argonne National Laboratory ("Argonne"). Argonne, a U.S. Department of Energy Office of Science laboratory, is operated under Contract No. DE-AC02-06CH11357. The U.S. Government retains for itself, and others acting on its behalf, a paid-up nonexclusive, irrevocable worldwide license in said article to reproduce, prepare derivative works, distribute copies to the public, and perform publicly and display publicly, by or on behalf of the Government.

* Corresponding author.

E-mail address: fangyan@anl.gov (F. Yan).

readily penetrate into the deep lung and initiate cardiopulmonary disease (Delfino et al., 2005; Pope and Dockery, 2006). Therefore, it is critical to know the size distribution of PM in the atmosphere, which is dependent both on the size distribution of primary PM and of secondary PM formed in the atmosphere.

Most current climate and chemical transport models have the ability to represent the temporal and spatial variability of the aerosol particle mass distribution but must assume a size distribution for the primary PM emissions in order to calculate radiative effects (Bauer et al., 2010) and transport. Most widely-used PM emission inventories (Bond et al., 2004; Cooke et al., 2002, 1999; Reff et al., 2009; Zhang et al., 2007) have very little size resolution and typically provide only mass emission information. Emission inventories for the U.S. (e.g., the National Emission Inventory (NEI)) and for Europe (e.g., European Monitoring and Evaluation Programme (EMEP)), as well as a few other countries, such as China (e.g., Zhang et al., 2007), provide some size information, but none of them provide continuous size distributions. They contain only very broad size bins such as total suspended particles (TSP), PM₁₀, and PM_{2.5}. Thus, modelers have to choose what sizes to assign for emission fluxes most of the time. The assumed size distributions may introduce a large amount of uncertainty in prediction of CCN concentrations (Pierce and Adams, 2009; Pierce et al., 2007; Reddington et al., 2013; Spracklen et al., 2011) and estimates of climate forcing (Bauer et al., 2010; Spracklen et al., 2011).

In this study, we develop the first global emission inventory of PM₁₀ with detailed particle size distribution, especially for submicron particles, and thereby advance our understanding of the effects of particle size. We acknowledge that number size distribution is also important and provides different information from mass size distribution. In this study, we provide size-resolved emissions by mass, since it can be applied directly to currently available PM emission inventories (Bond et al., 2004; Streets et al., 2004; Yan et al., 2014b, 2011; GAINS, 2014) without any modification to their calculation methodologies. We tabulate size distribution profiles from the literature that contain measured size distributions of particle emissions from each source category. Section 2 introduces the methodology used to parameterize the size distributions. Section 3 discusses the size distributions by region, energy sector, and designed scenarios. Conclusions and future work are summarized in Section 4.

2. Methodology and datasets

The size-resolved mass emission inventory in this work is built upon previous work (Bond et al., 2004) that involved coarse or no size resolution. In that work, a technology-based model was constructed to estimate present-day global emissions of black and organic carbon particles. This model determines emissions by apportioning fuel use among different emitting technologies. Such an approach has also been used for historical and future emissions estimates (Bond et al., 2007; Streets et al., 2004; Yan et al., 2014b, 2011). The technology-based model allows us to discriminate size distributions among sources with different technologies, as well as to keep track of their impacts. In this work, we use updated combinations of fuels, combustion technologies, and emission control technologies based on Bond et al. (2004) and apply appropriate size distributions for each combination.

Fig. 1 shows the framework for building a size-resolved emission inventory. First, this work enhances existing compilations through literature review and update. Particle size distributions by sector, fuel, and technology are collected from the literature, as detailed in the Supporting information (SI). Second, these distributions are parameterized by unimodal or multimodal lognormal distributions, depending on the sample size of each distribution and the

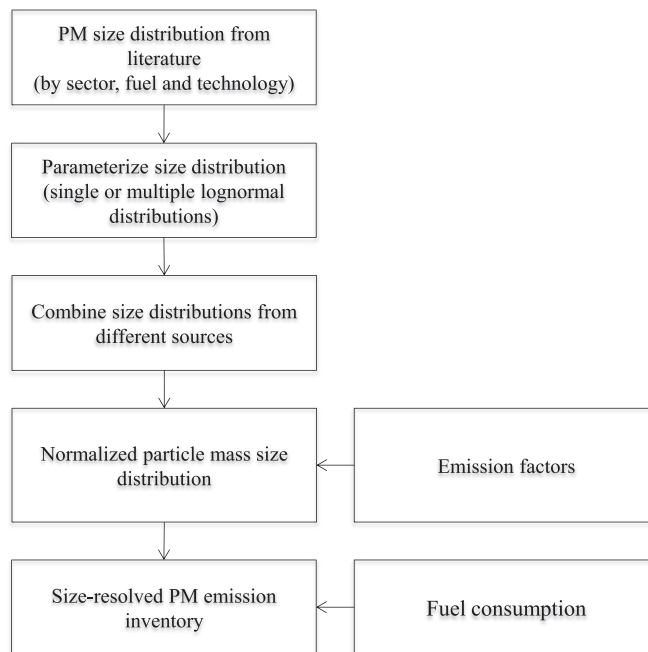


Fig. 1. Framework for building a size-resolved PM emission inventory.

availability of data, and presented as mass median diameters (MMD), geometric standard deviation (GSD), and mass mixing ratio or weight (*w*) within each mode, if the distribution has more than one mode, as shown in Section 2.2. The modeled size distributions do not reproduce the measurements exactly, so there is uncertainty in the derived parameters, as described in Section 2.3. Third, these size distributions from different data sources are merged. There are insufficient data available to use region-specific measurements. We choose to combine data from all regions to generate a more robust representation of the distribution for a particular technology. When more than one distribution for a single technology is included, these distributions are treated equally and the average of the distributions is used. Finally, the estimated size distributions of each technology are combined with the corresponding mass-based particle emission factors and a fuel consumption activity database to develop a size-resolved emission inventory. The resulting emission inventory gives a continuous mass distribution by particle size. The distribution of total PM₁₀ emissions (*Em*) along the logarithm of particle diameter ($\ln D_p$) for each sector *k* in a specific year *i* is given by:

$$Em_{i,k}(\ln D_p) = \sum_j \sum_l \sum_m FC_{i,j,k,l,m} EF_{k,l,m} g_{k,l,m}(\ln D_p) \quad (1)$$

where *i*, *j*, *k*, *l*, and *m* represent year, region, sector, fuel, and fuel/technology combination, respectively. *Em* is emission, *FC* is fuel consumption (kg/year), *EF* is emission factor (g/kg fuel) specific to a fuel/technology combination (including the effect of any control devices), *D_p* is particle diameter, and *g* ($\ln D_p$) is the particle size distribution of PM₁₀ in the form of a single- or multi-lognormal distribution (see Section 2.2).

Mass fractions within certain size bins (e.g., PM₁, PM_{1–2.5}, and PM_{2.5–10}) can also be computed by the integrals of the distribution. Using PM_{1–2.5} as an example, it can be estimated by:

$$MF_{a,b} = \frac{\int_{\ln(10)}^{\ln b} Em(\ln D_p)}{\int_{-\infty}^{\ln a} Em(\ln D_p)} \quad (2)$$

where MF is the mass fraction, $a = 1 \mu\text{m}$, and $b = 2.5 \mu\text{m}$.

2.1. Database of size distributions

We separate particle-size distributions based on different combinations of fuel, sector, and technology. The reasons are: (1) the particle-size distributions are diverse for different combustion and emission control technologies; (2) we can keep track of the individual contributions of particle-size distribution from each technology and thus have a better picture of the effects of emission control strategies; and (3) the grouping of technologies is consistent with our previous emission inventory, which enables us to apply the existing database of emission factors and corresponding activity levels. The size distribution information for all combustion sources used in this study is provided in the *SI*, where we discuss the development of the size-distribution information database. The discussion in *SI* also includes the review of size distribution data for important sources (large PM_{10} contributors) in the residential, industrial, power, and transportation sectors. It should be noted that size distribution information is not available for a few combustion sources; in such cases, we selected the size distribution of similar sources (similar combustion or fuel types, etc.) to represent those sources for which data are not available.

2.2. Parameterization of size distribution

A lognormal distribution often provides a good fit to the particle-size distribution and is commonly used in atmospheric studies (Aitchison and Brown, 1957; Friedlander, 1977; Whitby, 1974). Extensive discussions of the use of lognormal distributions for representing aerosols can be found in the literature (e.g., Hinds, 1998 and Seinfeld and Pandis, 2006). The particle-size distribution for a single mode, expressed as the mass of particles (M) per logarithmic size ($\ln D_p$) interval, can be formulated as:

$$\frac{dM}{d \ln D_p} = \frac{M_t}{\sqrt{2\pi} \ln \sigma_g} \exp \left[-\frac{(\ln D_p - \ln \bar{D}_{pg})^2}{2 \ln^2 \sigma_g} \right] \quad (3)$$

where D_p is the particle diameter, \bar{D}_{pg} is the mass median diameter (MMD), σ_g is the geometric standard deviation (GSD) of the distribution, and M_t is the total aerosol mass concentration. This study provides MMD information because it is then easier to represent the combination of size distribution and mass-based emission inventory. Count median diameter (CMD) is usually used by climate modelers and it can be converted using the Hatch-Choate relationship:

$$MMD = CMD \exp(3 \ln^2 \text{GSD}) \quad (4)$$

Due to the complex particle formation mechanisms and the variety of subsequent processes that occur prior to emission, the particle-size distribution may be characterized by more than one mode. For example, the mass distribution is usually dominated by two modes: the accumulation mode (from ~ 0.1 to $\sim 2 \mu\text{m}$) and the coarse mode (from ~ 2 to $\sim 50 \mu\text{m}$) (Seinfeld and Pandis, 2006). Particle-size distribution features with multiple modes can be described as the sum of lognormal distributions:

$$\frac{dM}{d \ln D_p} = M_1 f_1(\ln D_p) + M_2 f_2(\ln D_p) + \dots + M_k f_k(\ln D_p) \quad (5)$$

where k is the number of components in the mixture distribution, with $f_k(\ln D_p)$ being the lognormal distribution for mode k :

$$f_k(\ln D_p) = \frac{1}{\sqrt{2\pi} \ln \sigma_{gk}} \exp \left[-\frac{(\ln D_p - \ln \bar{D}_{pgk})^2}{2 \ln^2 \sigma_{gk}} \right] \quad (6)$$

Equation (6) can be normalized by the total mass concentration $M_t = \sum_{i=1}^k M_i$, so that the fitted curve of particle-size distribution is independent of the measured total mass, and the area under the curve ($\ln D_p$ from $-\infty$ to $+\infty$, or D_p from 0 to $+\infty$) is equal to 1. The normalized particle size distribution by mass can be expressed as:

$$g(\ln D_p) = w_1 f_1(\ln D_p) + w_2 f_2(\ln D_p) + \dots + w_k f_k(\ln D_p) \quad (7)$$

where $w_k = M_k / \sum_{i=1}^k M_i$ is the mass fraction of the f_k in the mixture distribution and termed “mixing weight” in this study.

Equation (7) is applicable to TSP, because this distribution is assumed to cover all particle sizes. Equation (8) is needed if an emission factor for a specific size of particle is applied. In this study, emissions of PM_{10} are used, and the adjustment is expressed as:

$$g'(\ln D_p) = \alpha [w_1 f_1(\ln D_p) + w_2 f_2(\ln D_p) + \dots + w_k f_k(\ln D_p)] \quad (8)$$

where α is the adjusted ratio that can be computed as

$$\alpha = 1 / \int_{-\infty}^{\ln D_{pt}} g(\ln D_p) d \ln D_p \quad \text{with } D_{pt} \text{ being the target particle size and } D_{pt} = 10 \mu\text{m in this study.}$$

In this work, we apply the method of nonlinear least-squares when fitting the measured data from reference materials. To obtain the coefficient estimates, the least-squares method minimizes the summed square of residuals. We use the curve-fitting toolbox from Matlab to fit published data on mass size distribution and estimate the mixing weight for each mode (w), MMD (\bar{D}_{pg}), and GSD (σ_g) with the nonlinear model described in Equations (6) and (7).

2.3. Uncertainties in size distribution

Uncertainties in fuel consumption activity and emission factors of PM are widely acknowledged and quantified in several studies (Lu et al., 2011; Yan et al., 2014a; Zhao et al., 2011), but few attempts have been made to examine uncertainties in the particle size distribution. In this work, we use nonlinear regression to parameterize size distribution, as described in Section 2.2. Uncertainties are introduced by fitting curves, which do not reproduce measured values exactly. In this work, we only consider the uncertainty due to fittings of lognormal distributions. Uncertainties caused by different measurements for the same technology are not included. The non-simultaneous prediction bounds for the function at a single predictor value $\ln D_{p,0}$ are quantified by:

$$P(\ln D_{p,0}) = g(\ln D_{p,0}) \pm t_{\alpha/2, n-m} \sqrt{\ln D_{p,0} S \ln D_{p,0}^T} \quad (9)$$

where t depends on the confidence level ($1 - \alpha$) and is computed using the inverse of the Student's t -test cumulative distribution function, n is the number of observations, m is the number of coefficients, and S is the covariance matrix of the coefficient estimates.

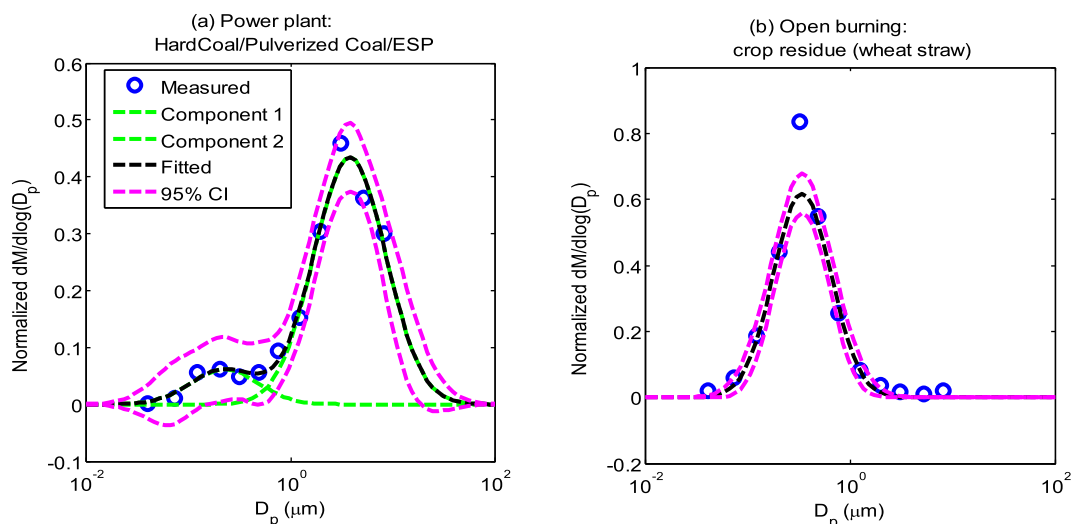


Fig. 2. Normalized particle size distribution by mass for: (a) power-plant boiler using pulverized coal and ESP emission control; and (b) open burning of wheat straw. Measured data, fitted curve, and 95% CI are shown. Data sources: Zhao et al. (2010) and Li et al. (2007).

Fig. 2 shows two examples of PM_{10} size distribution by mass: one is from a power plant boiler with ESP (Zhao et al., 2010), and the other is from the open burning of wheat straw (Li et al., 2007). The size distributions of PM_{10} given in both references were measured by an electrical low-pressure impactor (ELPI). This instrument operates in the size range of 0.03–10 μm , with 12 stages. Fig. 2 presents the parameterization of the size distribution, as well as the 95% confidence interval (CI) of the predicted curve. The size distribution of PM_{10} emissions from the boiler fits a curve with two lognormal distributions and MMDs of 0.2 μm and 3.8 μm , while the one from open burning of crop residue fits a single lognormal distribution with MMD of 0.3 μm . The width of the 95% CI indicates a larger uncertainty for the smaller particles if the simulated curve is used to predict size distributions for PM_{10} emissions from boilers with ESP. This kind of analysis is performed for all fuel and technology combinations.

We then use a Monte Carlo approach to determine the uncertainties in the size distribution of total emissions by sector and region. The procedure is to generate a set of random values of size distributions at $P(\ln D_{p,0})$ for specific particle diameter ($\ln D_{p,0}$) of each fuel/technology combination. We assume normal distributions for the predicted values $P(\ln D_{p,0})$, and standard deviation is estimated by $\sqrt{\ln D_{p,0} S \ln D_{p,0}^T}$ which depends on the particle size.

2.4. PM_{10} emission inventory

The PM_{10} emission inventory used in this study is based on previous studies (Bond et al., 2007, 2004; Lu et al., 2011; Streets et al., 2009, 2006; Yan et al., 2014b, 2011). Emission rates change widely due to different types of processes and control technologies, and therefore a technology-based methodology is necessary for estimating emissions from all anthropogenic combustion sources. Emission sources are categorized into four major sectors, including residential, industrial, power, and transportation, and more than 90 combinations of sector, fuel, and technology. Energy and fossil-fuel consumption data in 2010 for different combinations of sector, fuel, and technology are derived from International Energy Agency statistics (IEA, 2012a, 2012b). The fuel consumption activities are separated and aggregated based on the emission characteristics of each combustion process to fit the source types in our emission inventory (see Bond et al. (2004) for details). In particular, we

separate fuel consumption for on-road vehicles and agricultural tractors by emission standards (see Yan et al. (2014b) for details). We apply TSP emission factors from Bond et al. (2004, 2007) combined with the mass fractions of PM_{10} to TSP from the GAINS model (GAINS, 2014) to estimate PM_{10} emission factors, except for on-road vehicles and agricultural tractors which use primary TSP emission factors from Yan et al. (2014b) and the mass fraction of PM_{10} to TSP from Norbeck et al. (1998). Finally, fuel consumption activities for each set of sector, fuel, and technology and their corresponding emission factors are combined to estimate total emissions, as shown in Table 1.

3. Results and discussion

Regional size-resolved emissions for each sector are presented in Section 3.1 where we discuss the primary sources that dominate the emission size distribution by mass. Then, we compute emissions across all source types and present the global PM_{10} emission size distributions for all sectors in Section 3.2. Finally, in Section 3.3, we discuss the potential shifts in PM size that would be caused by the implementation of certain improved emission control technologies.

3.1. Regional size-resolved PM_{10} emissions

In this section we discuss the drivers of the size distribution patterns and uncertainties in each sector based on regional emissions. Sources that dominate mass emissions also dominate the size distribution, so that regions with similar emission contributions from the various sources also share similar size distributions. Representative regions are chosen for illustration and discussion. The selection of these regions is based on size distribution, such as number and position of peaks, and large mass contribution to global emissions and uncertainty.

3.1.1. Residential sector

Because solid fuels produce most of the PM_{10} in the residential sector, the size distribution of PM_{10} is dominated by the combustion of solid fuels. We present size distributions for OECD Europe, India, and China to represent characteristic distribution patterns of major emission sources in the residential sector where different technologies dominate, as shown in Fig. 3. In OECD Europe, PM_{10}

Table 1
Regional PM₁₀ emissions in 2010 (Gg/yr).

Region	Baseline				Scenario		
	Residential	Industry	Power	Transportation	Residential (S1 ^a)	Industry (S2 ^a)	Transportation (S3 ^a)
Canada	98	149	26	35	2	137	28
USA	495	820	515	239	36	753	198
Central America	372	334	61	339	22	283	270
South America	396	1676	76	314	27	1566	113
Northern Africa	39	366	11	233	10	270	124
Western Africa	1559	344	3	102	90	321	78
Eastern Africa	808	94	2	48	42	84	25
Southern Africa	574	195	41	148	31	177	104
OECD Europe	812	1332	762	334	56	1161	225
Eastern Europe	472	401	356	80	12	357	35
Former USSR	271	1154	227	174	28	1068	95
Middle East	264	909	213	319	10	687	140
South Asia (no India)	706	203	10	73	37	162	41
India	2491	1411	107	169	126	1190	61
East Asia (no China)	111	614	80	142	25	542	88
China	4392	10,672	380	551	188	8840	370
Southeast Asia	1535	976	67	347	70	817	209
Oceania	52	127	69	37	2	117	24
Japan	22	693	100	44	4	641	35
World	15,471	22,471	3107	3730	819	19,174	2263

^a S1 is the clean household-fuels combustion scenario; S2 is the controlled cement kiln scenario; S3 is the clean vehicle scenario.

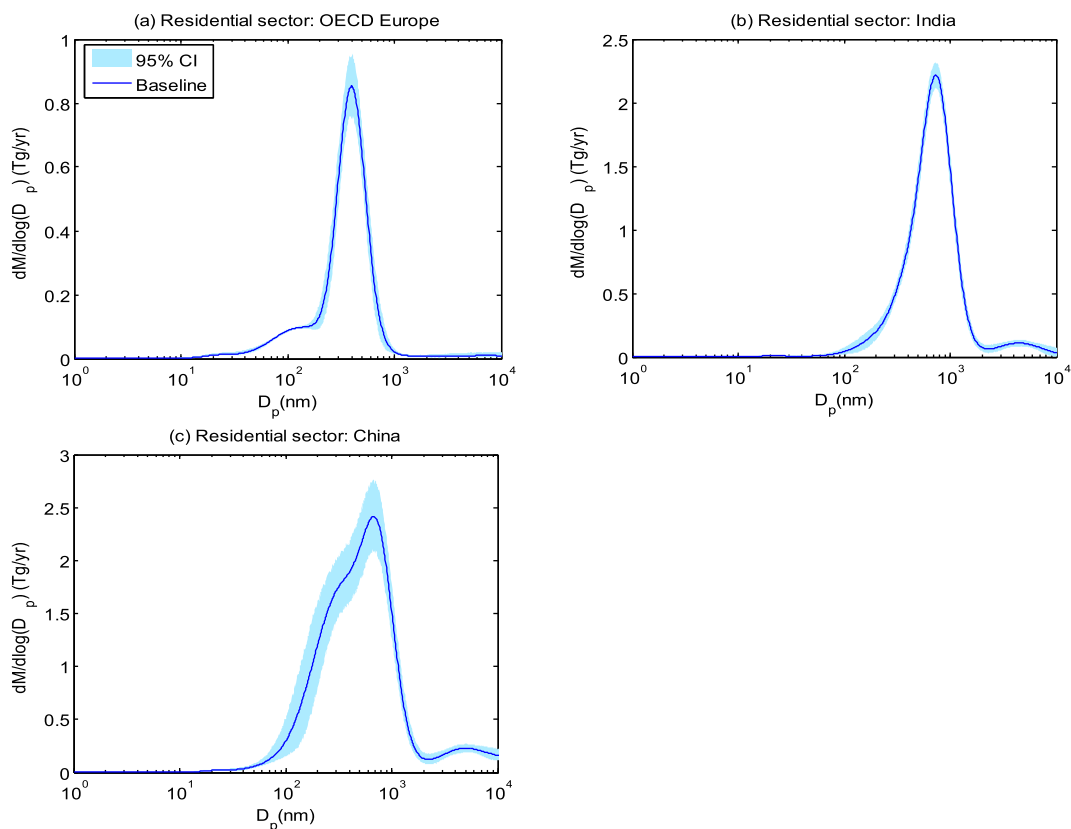


Fig. 3. Regional size-resolved PM₁₀ emissions with 95% CI for the residential sector for (a) OECD Europe, (b) India, and (c) China.

emissions typically show a bimodal distribution having peaks at around 100 nm and 400 nm. These two modes are primarily contributed by fireplaces and heating stoves. Bimodal distributions are also found in emissions from India. Emissions from agricultural waste, dung, and biomass cookstoves are the major sources of PM₁₀ emissions in the range of 50–2000 nm with a peak at 700 nm. The other peak at 4000–5000 nm is due to PM emissions from

traditional cookstoves burning hard coal. Uncertainties around the peak in OECD Europe and India are due to uncertainties in the estimated size distribution for heating stoves. In China, PM₁₀ emissions show a trimodal distribution. The peak at 300 nm is from combustion of hard coal in open fires. The other two peaks at 600 nm and 5000 nm are caused by combustion of fuelwood, agricultural waste, and hard coal in traditional stoves. Large

uncertainties in the estimated size distribution of particles smaller than 1000 nm are primarily associated with agricultural waste burning.

3.1.2. Industrial sector

Major emission sources in this sector are coal-fired kilns. Because emissions from industrial sources are dominated by coal combustion, the overall size distributions in this sector are similar among regions. Size distributions of emissions from the industrial sector in China and Southeast Asia are shown in Fig. 4. A single-peak distribution is the predominant size distribution for PM₁₀, while another peak, dominated by coking-coal combustion, is present beyond the PM₁₀ size range. In both regions, the primary emission source is cement kilns, which contribute the peak at 600 nm. In China, the coking-coal process primarily determines the shape of the distribution above 3000 nm. In Southeast Asia, other than cement kilns, another major source is traditional biofuel combustion, which gives rise to the peak at 600 nm. There is no peak beyond PM₁₀ in this region since coking-coal emissions are not significant. For both regions, emissions from cement kilns contribute most to the uncertainty of the size distribution. Smaller uncertainties are found in China for particles larger than 3000 nm and in Southeast Asia for particles smaller than 100 nm—because of lower uncertainties contributed by the coking-coal process and biofuel combustion, respectively.

3.1.3. Power plant sector

The primary emission source in the power sector is coal combustion. Some other fuels, such as natural gas and heavy oil, also contribute a small share to regional emissions. In this sector, we use the size distribution of emissions from OECD Europe and Eastern Europe to show the contribution from major emission sources, as presented in Fig. 5. In both regions, PM₁₀ emissions generally show a bimodal distribution but with different details. In OECD Europe, emissions peak at 200 nm and 2000 nm. The major contributors of the two peaks in this region are combustion of biofuels, pulverized-coal combustion with ESP, and waste combustion, which have bimodal distributions with MMDs at 160–300 nm and 2000–3000 nm. The major uncertainty of the size distribution in this sector is from pulverized-coal combustion with electrostatic precipitators. In Eastern Europe, major emissions and uncertainty sources are from pulverized-coal combustion with cyclone collectors and ESP.

3.1.4. Transportation sector

The size distribution of PM₁₀ in the transportation sector is

dominated by the combustion of diesel fuel. On-road vehicles, non-road engines, and international shipping are major PM emission sources in 2010. The size distributions for this sector are presented in Fig. 6. In the three regions selected—the U.S., Southern Africa, and Southeast Asia—multi-mode mass distributions having a major peak between 100 nm and 200 nm are typical characteristics of the transportation sector. This peak is contributed primarily by two-stroke engines, heavy-duty diesel vehicles, and heavy-fuel-oil combustion for international shipping. In the U.S., the peaks at 20 nm and 5000 nm are due to clean diesel vehicles meeting post-1998 emission standards and international shipping, respectively. Heavy-duty diesel vehicles without emission standards and two-stroke engines with poor maintenance are the major emission sources in Southern Africa, showing peaks at 50 nm and 150 nm. In Southeast Asia, the emission peaks at 20 nm, 150 nm, 1000 nm, and 5000 nm are primarily contributed by heavy-duty diesel vehicles without emission standards, superemitters, international shipping, and two-stroke engines. The large uncertainties for size distribution estimation in this sector are contributed by international shipping and vehicles without emission standards.

3.2. Global size-resolved PM emissions

Fig. 7 shows global size-resolved emissions from the four sectors: residential, industrial, power, and transportation. These four sectors exhibit dramatically different distributions. Residential emissions show a bimodal distribution with peaks at 600 nm and 5000 nm. These peaks are determined by the size distributions of emissions from solid-fuel combustion. In the industrial sector, PM₁₀ emissions show a peak at around 600 nm contributed primarily by emissions from kilns in the developing world, i.e., cement, lime, and brick kilns. Emissions from the combustion of solid fuels and waste in the power sector dominate the size distribution and lead to two peaks at 200 nm and 2000 nm. In the transportation sector, one peak is found between 100 and 200 nm governed by emissions from vehicles and international shipping, with three other peaks at 20 nm, 1000 nm, and 6000 nm. PM₁₀ emissions from the residential and transportation sectors tend to be of smaller size than those from the industrial and power sectors, since particles resulting from coal combustion, which is a major source in the industrial and power sectors, tend to be larger than those from biomass combustion in the residential sector and gasoline and diesel combustion in the transportation sector. Global emissions and regional contributions are summarized in Table 2. In the residential sector, we find that 86% of total PM₁₀ by mass is PM₁, while PM_{2.5–10} contributes only 4% of total PM₁₀ emissions. For

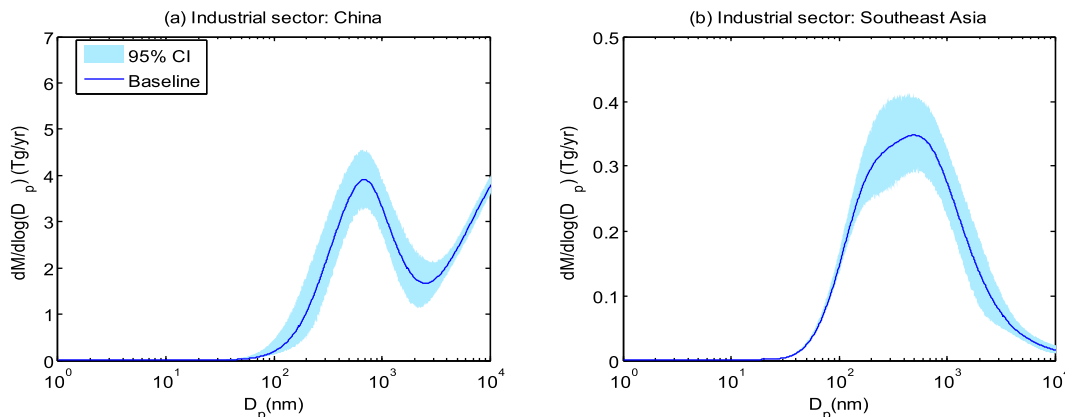


Fig. 4. Regional size-resolved PM₁₀ emissions with 95% CI for the industrial sector for (a) China and (b) Southeast Asia.

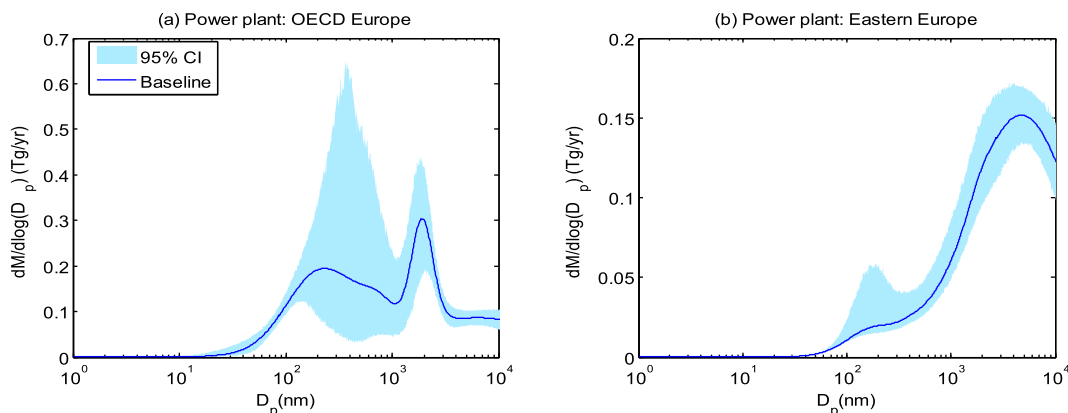


Fig. 5. Regional size-resolved PM₁₀ emissions with 95% CI for the power sector for (a) OECD Europe and (b) Eastern Europe.

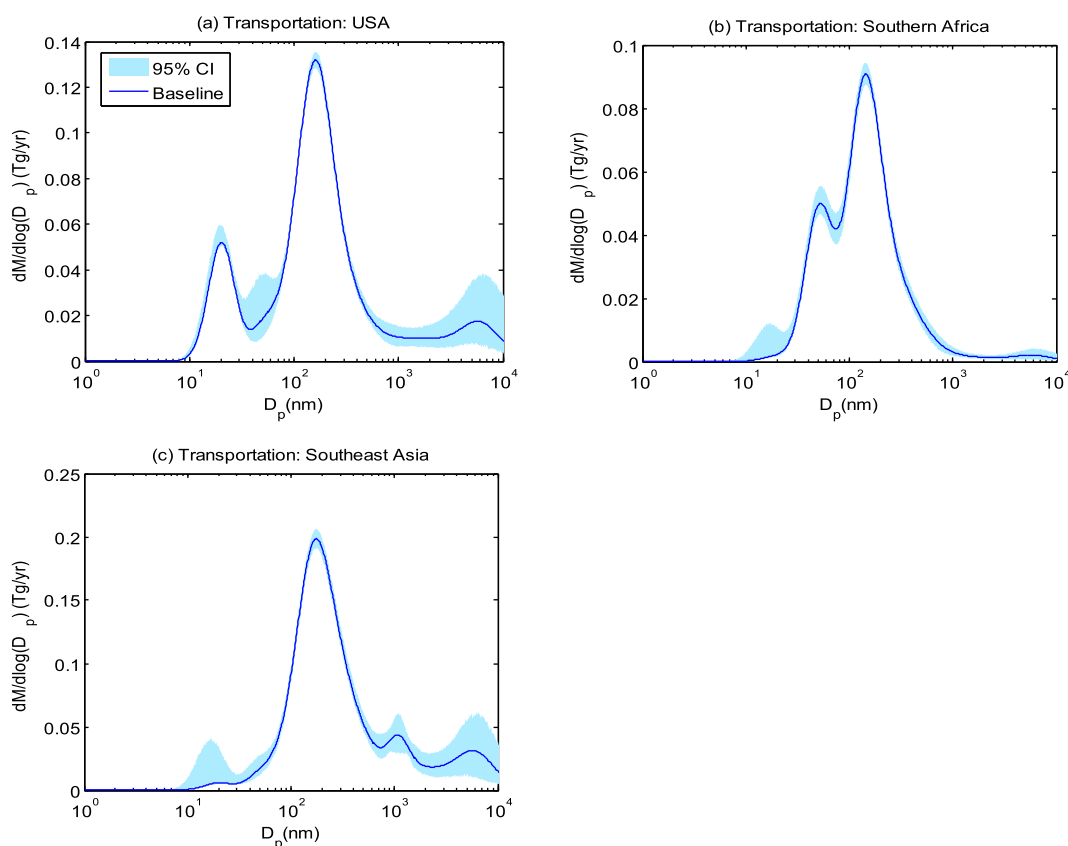


Fig. 6. Regional size-resolved PM₁₀ emissions with 95% CI for the transportation sector for (a) the U.S., (b) Southern Africa, and (c) Southeast Asia.

transportation, 92% of PM₁₀ is smaller than 1 μm and 5% of total emissions fall between PM₁₀ and PM_{2.5}. By contrast, in the industrial and power sectors, 54% and 42% of total emissions are contributed by PM₁, respectively. PM_{2.5–10} contributes 28% and 33%, and PM_{1–2.5} contributes 18% and 26%, respectively. Large uncertainties are found in the particle size range between 100 nm and 1000 nm for the residential, industrial, and power sectors, while small uncertainties are found in this particle size range for the transportation sector.

The global size-resolved emission distribution across all regions is presented in Fig. 8. This global average shows a single-mode lognormal distribution with peaks at 600–700 nm, reflecting the fact that global size-resolved PM₁₀ emissions are dominated by the

industrial and residential sectors, as shown in Fig. 8(a). PM_{2.5} and PM₁ contribute 82% and 67%, respectively, to total global PM₁₀ emissions. The majority of PM₁₀ emissions are from combustion sources yielding particles smaller than 1 μm . Fig. 8(b) shows the global size distribution by world region. Global particulate emissions are dominated by emissions in China, which contribute 36%, 33%, and 31% of global PM₁₀, PM_{2.5}, and PM₁, respectively. The ratios of regional to global PM emissions do not change much for PM₁₀, PM_{2.5}, and PM₁ in each region, suggesting that all regions contribute roughly the same fractions of PM₁₀ emissions in the different size ranges. Uncertainties in size-resolved emissions are larger in the particle size range between 100 nm and 5000 nm than in other size ranges.

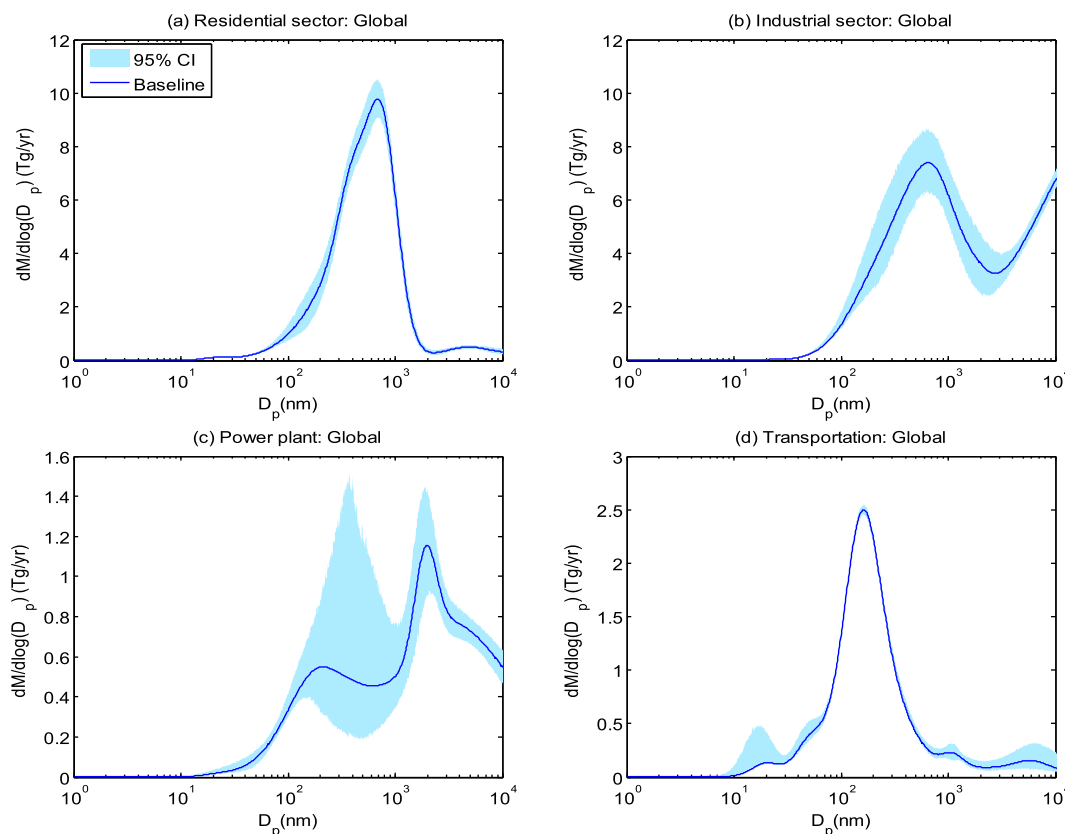


Fig. 7. Global size-resolved PM₁₀ emissions with 95% CI for (a) residential, (b) industrial, (c) power, and (d) transportation sectors.

3.3. Emission scenarios

In this section we examine the potential effects of adopting a higher level of PM emission control on the global PM₁₀ size distribution. In doing this, we focus more on changes in the size distribution pattern than in the overall magnitude of PM₁₀ emissions. We also do not pass judgment on the feasibility of these scenarios—they serve purely to illustrate the shifting size patterns. Three scenarios focusing on three major global PM₁₀ sources are investigated:

- (1) Clean household-fuel combustion scenario (S1). In this scenario, no solid fuel is used for cooking and heating in the home—it is substituted by LPG and natural gas, respectively.
- (2) Controlled cement kiln scenario (S2). In this scenario, baghouses are used to control emissions from all cement kilns, which are the major emission contributors in the industrial sector; the size-specific emission reduction profile assumed for this technology is 32% for PM₁₀ and 40% for PM_{2.5} (Lei et al., 2011).
- (3) Clean vehicle scenario (S3). In this scenario, it is assumed that all on-road vehicles meet Euro 6 emission standards and that no superemitters remain in the fleet.

The PM₁₀ regional emissions under the three scenarios are given in Table 1. Fig. 9 shows the global size distributions of PM₁₀ in the baseline and the three emission reduction scenarios. In scenario S1, as shown in Fig. 9(a), the size distribution shifts to a smaller size range with peaks at 20 nm and 200 nm. Compared with the baseline distribution, higher emissions of smaller particles are caused by increasing amounts of LPG and natural gas combustion.

Table 2
Global and regional PM₁₀, PM_{2.5–10}, PM_{2.5}, PM_{1–2.5}, and PM₁ emissions.

	PM ₁₀	PM _{2.5–10}	PM _{2.5}	PM _{1–2.5}	PM ₁
<i>Baseline emissions (Gg/yr)</i>					
Residential sector	15,471	588	14,883	1593	13,291
Industrial sector	22,471	6386	16,085	4016	12,069
Power sector	3107	1014	2093	797	1296
Transportation sector	3730	173	3556	132	3425
<i>Scenario emissions (Gg/yr)</i>					
Residential sector (S1 ^a)	819	1	818	8	811
Industrial sector (S2 ^a)	19,174	6332	12,843	3245	9597
Transportation sector (S3 ^a)	2263	172	2091	83	2009
<i>Regional contribution to global baseline emissions (%)</i>					
Canada	0.7	0.7	0.7	0.4	0.8
USA	4.6	4.1	4.7	4.2	4.9
Central America	2.5	0.9	2.8	1.8	3.0
South America	5.5	3.3	6.0	4.5	6.3
Northern Africa	1.5	0.5	1.7	1.3	1.7
Western Africa	4.5	0.4	5.4	3.5	5.8
Eastern Africa	2.1	0.2	2.6	1.5	2.8
Southern Africa	2.1	0.9	2.4	1.7	2.6
OECD Europe	7.3	6.7	7.3	7.1	7.4
Eastern Europe	2.9	4.8	2.5	2.7	2.5
Former USSR	4.1	8.9	3.0	3.8	2.8
Middle East	3.8	3.4	3.9	4.2	3.8
South Asia (no India)	2.2	0.5	2.6	2.1	2.7
India	9.3	5.6	10.1	10.1	10.2
East Asia (no China)	2.1	3.7	1.8	2.3	1.6
China	35.7	48.0	33.0	40.4	31.4
Southeast Asia	6.5	1.7	7.6	5.9	8.0
Oceania	0.7	0.9	0.6	0.6	0.6
Japan	1.9	4.8	1.3	1.9	1.1

^a S1 is the clean household-fuels combustion scenario; S2 is the controlled cement kiln scenario; S3 is the clean vehicle scenario.

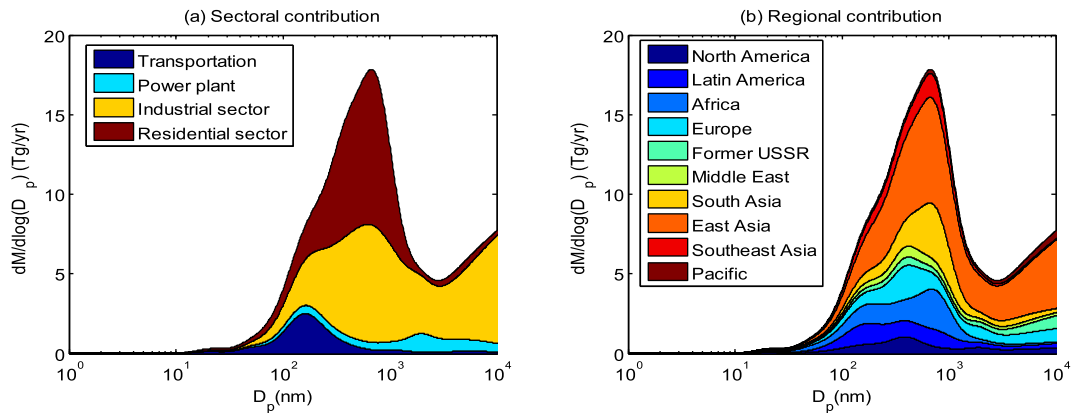


Fig. 8. Global size-resolved PM₁₀ emissions for all energy-related combustion sources: (a) emissions by sector; (b) emissions by major world region.

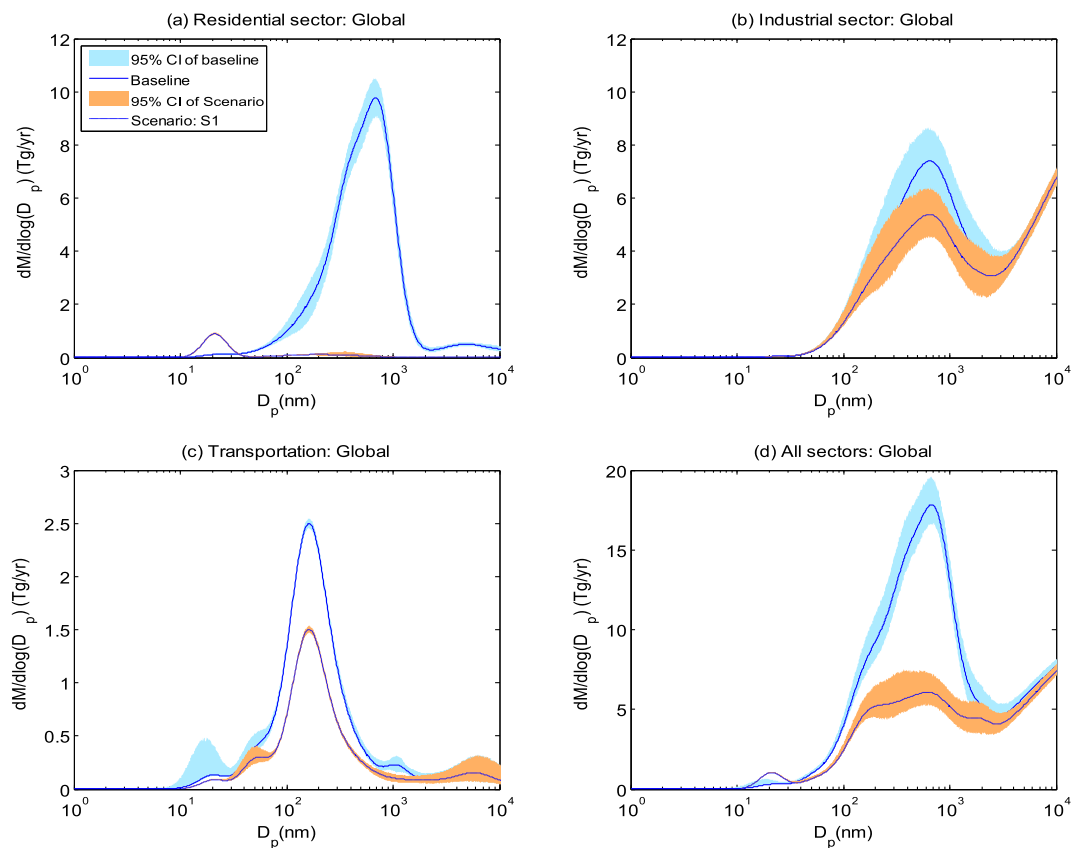


Fig. 9. Global size-resolved PM₁₀ emissions under assumed emission control scenarios: (a) clean household-fuels combustion scenario (S1), (b) controlled cement kiln scenario (S2), (c) clean vehicle scenario (S3), and (d) all control scenarios combined (S1 + S2 + S3).

In the range between 1 μm and 10 μm , the mass emissions shift from having peaks at 600 nm and 5000 nm in the baseline to 200 nm in S1, with a total mass reduction of 99%.

In scenario S2, shown in Fig. 9(b), there is no significant change in the shape of the size distribution, but PM emissions in size ranges smaller than 3000 nm and larger than 100 nm are reduced significantly, due to the performance of the baghouses. Overall, PM₁₀ emissions from the industrial sector are reduced by 15% from the baseline scenario. Emissions of PM_{2.5–10} are reduced by only 1% from the baseline, because the contribution of cement kilns to total emissions is much less than the contribution of the coking-coal

process for PM larger than 3000 nm. PM_{1–2.5} and PM₁ are reduced by 19–21%, with a significant reduction for PM larger than 100 nm, where emissions from cement kilns dominate the size distribution.

In scenario S3, forcing all vehicles to follow Euro 6 emission standards significantly reduces emissions of PM with sizes smaller than 2.5 μm . There is no change in the shape of the PM₁₀ size distribution from the baseline, except that a small peak at 50 nm emerges that is associated with the Euro 6 vehicles, as shown in Fig. 9(c). The overall emission reduction in the transportation sector is 39% with less than 1% change in PM_{2.5–10} from baseline.

Reductions of 37% and 41% are achieved in $PM_{1-2.5}$ and PM_1 , respectively.

If all of the measures described above were to be applied at the same time, total PM_{10} emissions would be reduced by 43% from the baseline. Although emissions of particles smaller than 100 nm increase, mainly due to the increase of emissions from LPG and natural gas combustion, mass emissions are less in all PM size ranges. $PM_{2.5-10}$, $PM_{1-2.5}$, and PM_1 are reduced by 8%, 37%, and 54%, respectively. Because emissions are reduced by a large amount in the residential sector, the global size distribution exhibits a different shape from the baseline. Four peaks are now observed in the global size distribution, contributed by the residential sector (at 20 nm and 2000 nm), the industrial sector (at 600 nm), and the transportation sector (at 20 nm and 200 nm).

4. Conclusions

In this work, we develop the first global and regional size-resolved PM_{10} mass emission inventory that covers all energy-related combustion sources. We collate particle size distribution information for all important types of combustion sources from the literature. Continuous size distributions across the full range of PM sizes less than PM_{10} are assembled for all combustion types, and PM emissions in three size ranges (PM_{10} , $PM_{2.5}$, and PM_1) and two size bins ($PM_{2.5-10}$ and $PM_{2.5-1}$) are summarized for the residential, industrial, power, and transportation sectors. The uncertainty associated with each size-resolved emission profile is also calculated. Global PM_{10} emissions from combustion sources are dominated by particle sizes smaller than 1 μm . PM_{10} emissions in the four sectors show different particle size distributions due to the different characteristics of the fuels and technologies used in each sector. In the residential and transportation sectors, 80–90% of emissions are smaller than 1 μm , with less than 5% of emissions from $PM_{2.5-10}$. In the industrial and power sectors, only 40–50% of emissions are in the PM_1 size range, while around 20–25% of emissions are in both $PM_{2.5-10}$ and $PM_{1-2.5}$. Three emission scenarios were studied to represent tighter emission limits in three sectors: switching from solid fuels to LPG and natural gas in the residential sector, installing baghouses to control emissions from cement kilns, and using Euro 6 emission limits for all in-use vehicles. Two of these scenarios show similar mass size distribution emission patterns as the baseline, while, in the residential sector, particle mass sizes are shifted to smaller size ranges. Despite the quantified uncertainties in this size-resolved PM_{10} emission database, its use in global and regional chemistry and climate models should be a great improvement over the rudimentary representations in current usage. This will, in turn, lead to improved quantification of human health and climate impacts. An evaluation of this size-resolved PM emission inventory through modeling and comparisons with observations is planned for the future. Additional measurements of size-resolved PM_{10} emissions from key combustion sources where data are presently limited would enable us to improve the distributions presented here.

Acknowledgments

This work was supported by the U.S. Environmental Protection Agency under grant RD-83503401. This paper has not been subject to EPA's required peer and policy review, and therefore does not necessarily reflect the views of the Agency. No official endorsement should be inferred. Argonne National Laboratory is operated by UChicago Argonne, LLC, under Contract No. DE-AC02-06CH11357 with the U.S. Department of Energy.

Appendix A. Supplementary data

Supplementary data related to this article can be found at <http://dx.doi.org/10.1016/j.atmosenv.2015.02.037>.

References

- Aitchison, J., Brown, J.A.C., 1957. The Lognormal Distribution Function. Cambridge University Press, Cambridge, UK.
- Anttila, T., Brus, D., Jaatinen, A., Hyvärinen, A.P., Kivekäs, N., Romakkaniemi, S., Komppula, M., Lihavainen, H., 2012. Relationships between particles, cloud condensation nuclei and cloud droplet activation during the third Pallas Cloud Experiment. *Atmos. Chem. Phys.* 12, 11435–11450.
- Bauer, S.E., Menon, S., Koch, D., Bond, T.C., Tsigaridis, K., 2010. A global modeling study on carbonaceous aerosol microphysical characteristics and radiative effects. *Atmos. Chem. Phys.* 10, 7439–7456.
- Bond, T.C., Bhardwaj, E., Dong, R., Jogani, R., Jung, S., Roden, C., Streets, D.G., Trautmann, N.M., 2007. Historical emissions of black and organic carbon aerosol from energy-related combustion, 1850–2000. *Glob. Biogeochem. Cycles* 21, GB2018.
- Bond, T.C., Streets, D.G., Yarber, K.F., Nelson, S.M., Woo, J.H., Klimont, Z., 2004. A technology-based global inventory of black and organic carbon emissions from combustion. *J. Geophys. Res.* 109, D14203.
- Cooke, W.F., Liousse, C., Cachier, H., Feichter, J., 1999. Construction of a 1×1 fossil fuel emission data set for carbonaceous aerosol and implementation radiative impact in the ECHAM4 model. *J. Geophys. Res.* 104, D18.
- Cooke, W.F., Ramaswamy, V., Kasibhatla, P., 2002. A general circulation model study of the global carbonaceous aerosol distribution. *J. Geophys. Res.* 107, D16.
- Delfino, R.J., Sioutas, C., Malik, S., 2005. Potential role of ultrafine particles in associations between airborne particle mass and cardiovascular health. *Environ. Health Perspect.* 113, 934–946.
- Feingold, G., 2003. Modeling of the first indirect effect: analysis of measurement requirements. *Geophys. Res. Lett.* 30, 19.
- Friedlander, S.K., 1977. Smoke, Dust and Haze, Fundamentals of Aerosol Behavior. John Wiley and Sons, New York, USA.
- GAINS, 2014. Greenhouse Gas – Air Pollution Interactions and Synergies (accessed June 2014). <http://gains.iiasa.ac.at/models/>.
- Haywood, J., Boucher, O., 2000. Estimates of the direct and indirect radiative forcing due to tropospheric aerosols: a review. *Rev. Geophys.* 38, 513–543.
- Hinds, W.C., 1998. Aerosol Technology. John Wiley & Sons, New York.
- International Energy Agency (IEA), 2012a. Energy Statistics of Non-OECD Countries CD-ROM Paris, France.
- International Energy Agency (IEA), 2012b. Energy Statistics of OECD Countries CD-ROM Paris, France.
- Lei, Y., Zhang, Q., Nielsen, C., He, K., 2011. An inventory of primary air pollutants and CO_2 emissions from cement production in China, 1990–2020. *Atmos. Environ.* 45, 147–154.
- Li, X., Duan, L., Wang, S., Duan, J., Guo, X., Yi, H., 2007. Emission characteristics of particulate matter from rural household biofuel combustion in China. *Energy Fuels* 21, 845–851.
- Lu, Z., Zhang, Q., Streets, D.G., 2011. Sulfur dioxide and primary carbonaceous aerosol emissions in China and India, 1996–2010. *Atmos. Chem. Phys.* 11, 9839–9864.
- McFiggans, G., Artaxo, P., Baltensperger, U., Coe, H., Facchini, M.C., Feingold, G., Fuzzi, S., Gysel, M., Fissic, D., Paulo, U.D.S., Matao, R., Travessa, R., Paulo, C.E.P.S., 2006. The effect of physical and chemical aerosol properties on warm cloud droplet activation. *Atmos. Chem. Phys.* 6, 2593–2649.
- Norbeck, J., Durbin, T., Truex, T., 1998. Measurement of Primary Particulate Matter Emissions from Light-duty Motor Vehicles. CRC Project No. E-24-2. <http://cichlid.cert.ucr.edu/research/pubs/98-ve-rt2a-001-fr.pdf> (accessed in December 2013).
- Pierce, J.R., Adams, P.J., 2009. Uncertainty in global CCN concentrations from uncertain aerosol nucleation and primary emission rates. *Atmos. Chem. Phys.* 9, 1339–1356.
- Pierce, J.R., Chen, K., Adams, P.J., 2007. Contribution of primary carbonaceous aerosol to cloud condensation nuclei: processes and uncertainties evaluated with a global aerosol microphysics model. *Atmos. Chem. Phys.* 7, 5447–5466.
- Pope, C.A., Dockery, D.W., 2006. Health effects of fine particulate air pollution: lines that connect. *J. Air Waste Manag. Assoc.* 56, 709–742.
- Reddington, C.L., McMeeking, G., Mann, G.W., Coe, H., Frontoso, M.G., Liu, D., Flynn, M., Spracklen, D.V., Carslaw, K.S., 2013. The mass and number size distributions of black carbon aerosol over Europe. *Atmos. Chem. Phys.* 13, 4917–4939.
- Reff, A., Bhawe, P.V., Simon, H., Pace, T.G., Pouliot, G.A., Mobley, J.D., Houyoux, M., 2009. Emissions inventory of $PM_{2.5}$ trace elements across the United States. *Environ. Sci. Technol.* 43, 5790–5796.
- Seinfeld, J.H., Pandis, S.N., 2006. Atmospheric Chemistry and Physics from Air Pollution to Climate Change, second ed. John Wiley & Sons, Hoboken, New Jersey.
- Spracklen, D.V., Carslaw, K.S., Pöschl, U., Rap, A., Forster, P.M., 2011. Global cloud condensation nuclei influenced by carbonaceous combustion aerosol. *Atmos. Chem. Phys.* 11, 9067–9087.
- Streets, D.G., Bond, T.C., Lee, T., Jang, C., 2004. On the future of carbonaceous aerosol emissions. *J. Geophys. Res.* 109, D24212.

- Streets, D.G., Wu, Y., Chin, M., 2006. Two-decadal aerosol trends as a likely explanation of the global dimming/brightening transition. *Geophys. Res. Lett.* 33, L15806.
- Streets, D.G., Yan, F., Chin, M., Diehl, T., Mahowald, N., Schultz, M., Wild, M., Wu, Y., Yu, C., 2009. Anthropogenic and natural contributions to regional trends in aerosol optical depth, 1980–2006. *J. Geophys. Res.* 114, D00D18.
- Whitby, K.T., 1974. Modeling of multimodal aerosol distributions. In: GAF Meeting, October 1974, Bad Soden, Germany.
- Yan, F., Winijkul, E., Bond, T.C., Streets, D.G., 2014a. Global emission projections of particulate matter (PM): II. Uncertainty analyses of on-road vehicle exhaust emissions. *Atmos. Environ.* 87, 189–199.
- Yan, F., Winijkul, E., Jung, S., Bond, T.C., Streets, D.G., 2011. Global emission projections of particulate matter (PM): I. Exhaust emissions from on-road vehicles. *Atmos. Environ.* 45, 4830–4844.
- Yan, F., Winijkul, E., Streets, D.G., Lu, Z., Bond, T.C., Zhang, Y., 2014b. Global emission projections for the transportation sector using dynamic technology modeling. *Atmos. Chem. Phys.* 14, 5709–5733.
- Yu, H., Kaufman, Y.J., Chin, M., Feingold, G., Remer, L.A., Anderson, T.L., Balkanski, Y., Bellouin, N., 2006. A review of measurement-based assessments of the aerosol direct radiative effect and forcing. *Atmos. Chem. Phys.* 6, 613–666.
- Zhang, Q., Streets, D.G., He, K., Klimont, Z., 2007. Major components of China's anthropogenic primary particulate emissions. *Environ. Res. Lett.* 2, 045027.
- Zhao, Y., Nielsen, C.P., Lei, Y., McElroy, M.B., Hao, J., 2011. Quantifying the uncertainties of a bottom-up emission inventory of anthropogenic atmospheric pollutants in China. *Atmos. Chem. Phys.* 11, 2295–2308.
- Zhao, Y., Wang, S., Nielsen, C.P., Li, X., Hao, J., 2010. Establishment of a database of emission factors for atmospheric pollutants from Chinese coal-fired power plants. *Atmos. Environ.* 44, 1515–1523.